

Surface plasmon enhanced giant Faraday effect in graphene

Yang Li · Ka-Di Zhu

Received: 4 June 2013 / Accepted: 24 October 2013 / Published online: 22 November 2013
© Springer-Verlag Berlin Heidelberg 2013

Abstract We have theoretically investigated the giant Faraday rotation effect in graphene coupled to metal nanoparticles (MNPs). MNP-induced Faraday rotation effect (MIFRE) results in a giant Faraday rotation angle in high-frequency region where usually no significant Faraday rotation would occur in graphene. Another advantage of MIFRE is the enhanced amplification of the rotating light beam. Furthermore, the MIFRE can be tuned by changing the MNP–graphene distance. The high efficiency and tunability of MIFRE in graphene predict its potential applications in novel graphene-based optical modulators and switches.

1 Introduction

In recent years, the optical properties of hybrid nanostructures involving metal nanoparticle (MNP), such as MNP-semiconductor quantum dot (SQD) [1, 2], MNP-nanocavity [3], MNP-solar cells [4] and MNP pairs [5], have attracted a lot of attention. Most recently, the strong plasmon-mediated interaction between two SQDs in a MNP-SQD hybrid system has been studied by Artuso et al. [6], while Kosionis et al. [7] have also demonstrated the optical features of this hybrid system under a weak probe field. They show that the QD-MNP coupling enables the energy flow from the metallic nanoparticle to the quantum dot. This flow leads to an amplified probe beam. In this

case, the hybrid nanostructures would find a broad range of potential applications in optical devices.

The MNP-graphene coupled system is one of the most interesting hybrid nanostructures. Hong et al. [8] have prepared gold nanoparticle-graphene composites by controlling the feeding weight ratio of both components and studied their applications in biosensors. The strong light scattering due to surface plasmon resonance on MNPs is employed as an effective signal reporter to illuminate the graphene sheet for optical imaging [9]. Li et al. [10] demonstrated that the Pd-graphene hybrid system can act as an efficient catalyst for the Suzuki reaction under the aqueous and aerobic conditions. Most recently, Zaniewski et al. [11] proposed a scheme of the MNP-filled graphene sandwiches lately. Though many experiments on properties of MNP-graphene hybrid system have been achieved in recent years, the influence of MNP on the optical Faraday rotation effect in graphene has not yet been investigated so far.

When a light propagates in a dielectric or metal with the presence of a static magnetic field along the propagation direction of the light, the polarization plane of light will rotate. This phenomena are generally referred to as optical Faraday rotation effect (FRE). The FRE can be utilized in diverse applications in optical telecommunications and laser technology, such as modulators, optical isolators, circulators, magnetic field sensing and spintronics [12, 13]. The giant Faraday rotation in graphene has been achieved in recent experiments [14, 15]. However, the Faraday rotation is large only in low frequency region and also reduces to zero in the higher frequencies. The significant FRE in higher frequency region has been achieved via nano-patterning in graphene [16]. Another important problem limited the practical utilizations of FRE is the low intensity of the output light due to the absorption of

Y. Li · K.-D. Zhu (✉)

Key Laboratory of Artificial Structures and Quantum Control
(Ministry of Education), Department of Physics and Astronomy,
Shanghai Jiao Tong University, 800 Dong Chuan Road,
Shanghai 200240, China
e-mail: zhukadi@sjtu.edu.cn

graphene, which can be relieved by using a Fabry-Perot cavity [17].

In the present work, we will investigate the modifications of FRE in graphene caused by Au nanoparticles theoretically. The giant Faraday rotation angles in high-frequency region are obtained, where usually no significant Faraday rotation would occur as compared with the conventional graphene FRE.

2 Theory

The schematic of the system is shown in Fig. 1a. The gold nanoparticle is embedded in the substrate on which is a monolayer graphene sheet. Then, a light beam propagates from the substrate to the graphene. The surface plasmon on Au nanoparticle should be excited by the beam. Thus, the interaction between Au nanoparticle and graphene can be created. Fig. 1b illustrates a typical graphene FRE. In general, graphene is a 2D hexagonal lattice with two carbon atoms per unit, forming two equivalent sublattices marked *A* and *B* (see Fig. 1c). The reciprocal lattice contains two lattice points as well, namely the so-called Dirac points (marked **K** and **K'**). The conduction and valence bands are in touch with each other at Dirac points. We assume that **K** and **K'** points could be dealt with separately (introducing a valley degeneracy $g_v = 2$), and the spin of electron comes into the problem as a spin degeneracy factor $g_s = 2$ since the Zeeman effect caused by the

external magnetic field ($B < 15T$) is not notable. Thus, we could just focus on the **K** valley whose Hamiltonian is

$$H_0 = v_F \boldsymbol{\sigma} \cdot \mathbf{P}, \quad (1)$$

where $\mathbf{P} = \mathbf{p} + e\mathbf{A}$, e is the electron charge and \mathbf{A} is the vector potential of electromagnetic field imposed on graphene. Given an external static magnetic field \mathbf{B} along z -axis and perpendicular to the graphene plane, i.e., xy -plane, we set the vector potential of \mathbf{B} as $\mathbf{A}_B = (0, Bx, 0)$, satisfying the relation $\mathbf{B} = \nabla \times \mathbf{A}_B$. Then, the eigenenergies and their eigenstates could be solved as

$$E_n = \text{sign}(n) \frac{\hbar v_F}{l_B} \sqrt{2|n|}, \quad n = 0, \pm 1, \pm 2, \dots \quad (2)$$

$$\phi_{n,k_y} = \begin{cases} \frac{1}{(2L)^{1/2}} e^{ik_y y} [\phi_{|n|-1}, i \text{sign}(n) \phi_{|n|}]^T, & n = \pm 1, \pm 2, \dots \\ \frac{1}{L^{1/2}} e^{ik_y y} [0, \phi_0]^T, & n = 0, \end{cases} \quad (3)$$

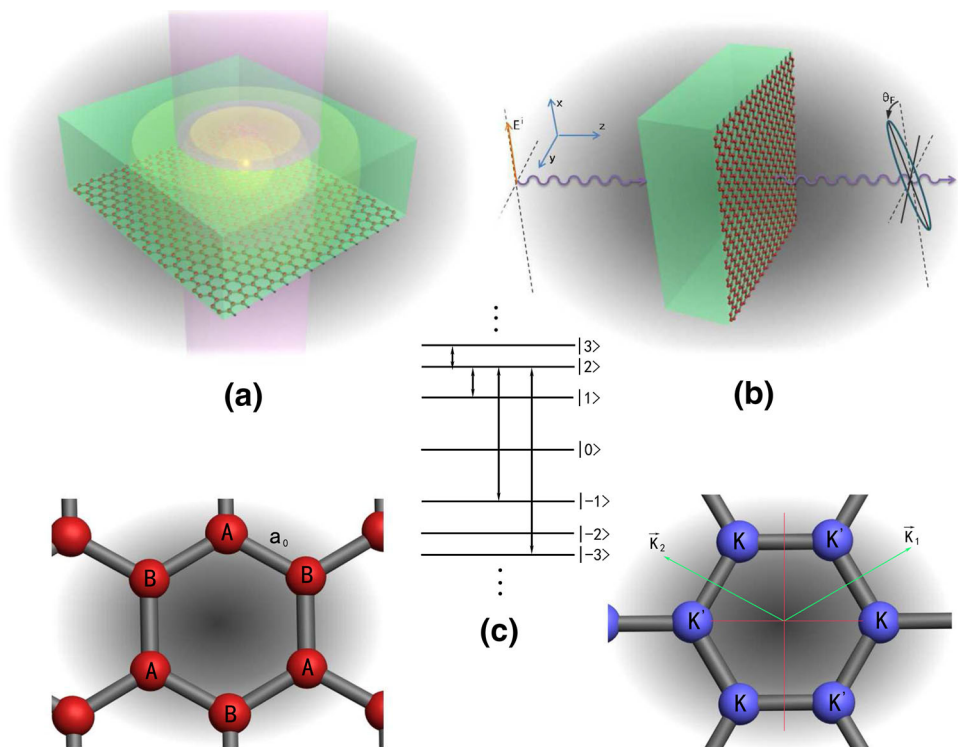
where $\phi_n = e^{-\frac{\zeta(x)^2}{2}} H_n(\zeta(x)) / \sqrt{n! 2^n l_B \sqrt{\pi}}$, $\zeta(x) = \frac{x}{l_B} + l_B k_y$, $l_B = \sqrt{\frac{\hbar}{eB}}$ could be referred to as magnetic length and $H_n(x)$ is the Hermite polynomial.

When an additional optical beam irradiates the monolayer graphene sheet, the Hamiltonian of this system should be

$$H = H_0 + ev_F \boldsymbol{\sigma} \cdot \mathbf{A}_p(\mathbf{t}), \quad (4)$$

where $\mathbf{A}_p(\mathbf{t}) = \mathbf{x} A_p(e^{-i\omega_p t} + e^{i\omega_p t})$ is vector potential of the added beam polarized along x -axis. We replace the vector

Fig. 1 **a** Schematic of the system consisting of a graphene sheet and Au-MNP embedded in the substrate. Both of them are irradiated by a laser beam. **b** Faraday rotation effect of the laser beam. **c** Lattice structure of graphene, Brillouin zone and the energy level structures of graphene in an external static magnetic field



potential with the beam itself for convenience, and then, H is

$$H = H_0 + \frac{e v_F}{\omega_p} E_p \sigma_x (e^{-i\omega_p t} + e^{i\omega_p t}), \tag{5}$$

where $E_p = \omega_p A_p$ is the equivalent electric field. As in Ref.[18], by executing a second-quantization process

$$H \rightarrow \langle \Psi_{k_y} | H | \Psi_{k_y} \rangle, \tag{6}$$

where $|\Psi_{k_y}\rangle = a_{0,k_y} |0, k_y\rangle + \sum_{n \geq 1} (c_{n,k_y} |n, k_y\rangle + v_{n,k_y} | -n, k_y\rangle)$, c_{n,k_y} is the annihilation operator obeying

fermionic anticommutation rules: $[c_{n,k_y}, c_{m,k'_y}^\dagger]_+ = \delta_{n,m} \delta_{k_y,k'_y}$

and $[c_{n,k_y}^\dagger, c_{m,k'_y}^\dagger]_+ = [c_{n,k_y}, c_{m,k'_y}]_+ = 0$ (a_{0,k_y} and v_{n,k_y} could be interpreted in exactly the same manner). Since the index k_y will not lead to any different results, it could be omitted in the following treatments safely and return in the last step. Therefore, the Hamiltonian can be written by

$$\begin{aligned} H = & \sum_{n \geq 1} (E_n c_n^\dagger c_n + E_{-n} v_n^\dagger v_n) - \mu_0 E_p (e^{-i\omega_p t} + e^{i\omega_p t}) \\ & \times (c_1^\dagger a_0 + v_1^\dagger a_0 + h.c.) \\ & - 2\mu E_p \cos(\omega_p t) i \sum_{n \geq 1} (c_n^\dagger v_{n+1} + c_{n+1}^\dagger v_n - c_{n+1}^\dagger c_n \\ & - v_n^\dagger v_{n+1} - h.c.), \end{aligned} \tag{7}$$

where $\mu_0 = -\frac{e v_F}{\sqrt{2}\omega_p}$ and $\mu = \frac{e v_F}{2\omega_p}$ are the equivalents of electric dipole moment.

Next, we introduce our main hypothesis. From Eq. (7), we should emphasize that only those between two levels (marked n and m) fulfilled the selection rule: $|n| - |m| = \pm 1$, could have the optical transitions (for instance, $n = 2$ is given in Fig. 1c). We postulate every two transition-permitted levels build up a two-level system, which interacts with optical fields independently and ignores the influences from the other levels. Taking the levels $|n\rangle$ and $| -n - 1\rangle$ (concerning $c_n^\dagger v_{n+1}$) as an example, then the Hamiltonian of the subsystem whose core is the two-level system formed by $|n\rangle$ and $| -n - 1\rangle$ can be described by

$$H_s = \hbar\omega S_z - \mu E_p (e^{-i\omega_p t} + e^{i\omega_p t}) i (S^+ - S^-), \tag{8}$$

where $\hbar\omega = E_n - E_{-(n+1)}$. S_z , S^+ and S^- indicate the ordinary pseudo-spin $-1/2$ operators. Obviously, H_s holds for the cases similar to $c_n^\dagger v_{n+1}$, such as $c_{n+1}^\dagger v_n$, $c_{n+1}^\dagger c_n$ and $v_n^\dagger v_{n+1}$, while the Hamiltonians of $c_1^\dagger a_0$ and $v_1^\dagger a_0$ cases read

$$H_{s0} = \hbar\omega S_z - \mu_0 E_p (e^{-i\omega_p t} + e^{i\omega_p t}) (S^+ + S^-). \tag{9}$$

When a MNP is included, the surface plasmon on MNP should be excited by the light beam, and then, an effective

field, which a two-level ‘‘atom’’ (TLA) actually feels, can be expressed as [19, 20]

$$\widetilde{E}'_p = E_p e^{-i\omega_p t} + \frac{S_z P_{Au}}{\epsilon_{\text{eff}1} d^3}, \tag{10}$$

$$P_{Au} = \varrho r_0^3 \left(E_p e^{-i\omega_p t} + \frac{S_z P_{\text{atom}}}{\epsilon_{\text{eff}2} d^3} \right), \tag{11}$$

where d is the distance between Au-MNP and graphene sheet, r_0 stands for the diameter of Au-MNP and S_z is the polar factor for electric field polarization, which is 2 in the present case. ϵ_b , ϵ_g and $\epsilon_{Au}(\omega_p) = 1 - \frac{\omega_{\text{spp}}^2}{\omega_p(\omega_p + i\gamma_{\text{spp}})}$ in which ω_{spp} and γ_{spp} represent the frequency and relaxation rate of the surface plasmon and denote the dielectric constants of background, graphene and Au-MNP, respectively. Then, $\epsilon_{\text{eff}1}$, $\epsilon_{\text{eff}2}$ and ϱ can be written as

$$\epsilon_{\text{eff}1} = \frac{2\epsilon_b + \epsilon_g}{3\epsilon_b}, \tag{12}$$

$$\epsilon_{\text{eff}2} = \frac{2\epsilon_b + \epsilon_{Au}(\omega_p)}{3\epsilon_b}, \tag{13}$$

$$\varrho = \frac{\epsilon_{Au}(\omega_p) - \epsilon_b}{2\epsilon_b - \epsilon_{Au}(\omega_p)}. \tag{14}$$

The dipole moment of a TLA can be expressed via the off-diagonal elements of the density matrix: $P_{\text{atom}} = \mu S^-$. Therefore, \widetilde{E}'_p should have the form

$$\widetilde{E}'_p = \eta E_p e^{-i\omega_p t} + \mu \zeta S^-, \tag{15}$$

where $\eta = 1 + \frac{\varrho r_0^3 S_z}{\epsilon_{\text{eff}1} d^3}$ and $\zeta = \frac{\varrho r_0^3 S_z}{\epsilon_{\text{eff}1} \epsilon_{\text{eff}2} d^6}$. Substituting \widetilde{E}'_p into H_s and H_{s0} , we achieve their revised versions, i.e.,

$$\begin{aligned} H'_s = & \hbar\omega S_z - \mu E_p (\eta e^{-i\omega_p t} + \eta^* e^{i\omega_p t}) i (S^+ - S^-) \\ & - i\mu^2 (\zeta S^- S^+ - \zeta^* S^+ S^-), \end{aligned} \tag{16}$$

$$\begin{aligned} H'_{s0} = & \hbar\omega S_z - \mu_0 E_p (\eta e^{-i\omega_p t} + \eta^* e^{i\omega_p t}) (S^+ + S^-) \\ & - \mu_0^2 (\zeta S^- S^+ + \zeta^* S^+ S^-). \end{aligned} \tag{17}$$

With the equation $\dot{A} = [A, H]/i\hbar$, we could derive the equations of motion for S^- , which are

$$\begin{aligned} i\hbar \dot{S}^- = & \hbar\omega S^- + 2i\mu E_p (\eta e^{-i\omega_p t} + \eta^* e^{i\omega_p t}) S_z - i\hbar \Gamma S^- \\ & + 2i\mu^2 (\zeta S^- S_z - \zeta^* S_z S^-), \end{aligned} \tag{18}$$

and

$$\begin{aligned} i\hbar \dot{S}^- = & \hbar\omega S^- + 2\mu_0 E_p (\eta e^{-i\omega_p t} + \eta^* e^{i\omega_p t}) S_z - i\hbar \Gamma S^- \\ & + 2\mu_0^2 (\zeta S^- S_z + \zeta^* S_z S^-), \end{aligned} \tag{19}$$

for H_s and H_{s0} respectively, where Γ is the dephasing rate introduced phenomenally. Applying the approximation in Ref. [18], $\langle S_z \rangle$ should replace S_z and provided $S_z =$

$(c_n^\dagger c_n - v_{n+1}^\dagger v_{n+1})/2$, $\langle S_z \rangle$ would be $[n_F(E_n) - n_F(E_{-(n+1)})]/2$ with $n_F(E) = 1/[1 + \exp(\frac{E-E_F}{k_B T})]$. Suppose $\langle S^- \rangle = S_+ e^{-i\omega_p t} + S_- e^{i\omega_p t}$, then we immediately obtain two sets of equations for H_s and H_{s0} , namely

$$\begin{cases} S_+ = 2i\mu E_p \eta \langle S_z \rangle / [-\hbar\omega + \hbar\omega_p + i\hbar\Gamma + 4\mu^2 \text{Im}(\zeta) \langle S_z \rangle], \\ S_- = 2i\mu E_p \eta^* \langle S_z \rangle / [-\hbar\omega - \hbar\omega_p + i\hbar\Gamma + 4\mu^2 \text{Im}(\zeta) \langle S_z \rangle], \end{cases} \tag{20}$$

and

$$\begin{cases} S_+ = 2\mu_0 E_p \eta \langle S_z \rangle / [-\hbar\omega + \hbar\omega_p + i\hbar\Gamma - 4\mu_0^2 \text{Re}(\zeta) \langle S_z \rangle], \\ S_- = 2\mu_0 E_p \eta^* \langle S_z \rangle / [-\hbar\omega - \hbar\omega_p + i\hbar\Gamma - 4\mu_0^2 \text{Re}(\zeta) \langle S_z \rangle]. \end{cases} \tag{21}$$

We define a operator set $\mathbb{P} = \{P_n^{(1)} = c_n^\dagger v_{n+1}, P_n^{(2)} = c_{n+1}^\dagger v_n, P_c = c_1^\dagger a_0, P_v = v_1 a_0^\dagger, P_n^{(3)} = c_{n+1}^\dagger c_n, P_n^{(4)} = v_n^\dagger v_{n+1}\}$. One cannot miss the relation: $P = S^+, \forall P \in \mathbb{P}$. Since it is an awfully complicated task to list the expressions for all the elements in \mathbb{P} which contains almost no significant physics as well, we just present two of them as instances. We absolutely have $P_n^{(1)} = P_n^{(1)}(\omega_p) e^{-i\omega_p t} + P_n^{(1)}(-\omega_p) e^{i\omega_p t}$ and $P_c = P_c(\omega_p) e^{-i\omega_p t} + P_c(-\omega_p) e^{i\omega_p t}$, then $P_n^{(1)}(\omega_p)$ and $P_c(\omega_p)$ could be solved by utilizing Eqs.(20) and (21), which are

$$\begin{cases} P_n^{(1)}(\omega_p) = S_-^* = \frac{\frac{e^2 F_A p \eta [n_F(E_{-(n+1)}) - n_F(E_n)]}{E_{-(n+1)} - E_n - \hbar\omega_p - i\hbar\Gamma + 2\mu^2 \text{Im}(\zeta) [-n_F(E_{-(n+1)}) + n_F(E_n)]}}{\sqrt{2} A_p \eta \frac{n_F(E_0) - n_F(E_1)}{E_0 - E_1 - \hbar\omega_p - i\hbar\Gamma - 2\mu_0^2 \text{Re}(\zeta) [-n_F(E_0) + n_F(E_1)]}}, \\ P_c(\omega_p) = S_-^* = \frac{e^2 F_A p \eta [n_F(E_{-(n+1)}) - n_F(E_n)]}{\sqrt{2} A_p \eta \frac{n_F(E_0) - n_F(E_1)}{E_0 - E_1 - \hbar\omega_p - i\hbar\Gamma - 2\mu_0^2 \text{Re}(\zeta) [-n_F(E_0) + n_F(E_1)]}}. \end{cases} \tag{22}$$

Evidently, if the Au-MNP is removed, i.e., $\eta \rightarrow 1$ and $\zeta \rightarrow 0$, Eq.(22) will reduce exactly the same as Eq.(36) and Eq.(37) in Ref.[18].

In order to demonstrate the influence of Au-MNP on the graphene FRE, we calculate the optical conductivity with $\sigma_{ij}(\omega) = g_v g_s \frac{\tilde{J}_i(\omega)}{E_j(\omega)}$. We employ a continuum description of current density operator with the form [21, 22]

$$\mathbf{J} = -\frac{e v_F}{S_A} \boldsymbol{\sigma}, \tag{23}$$

where $S_{\{A}}$ is the area of graphene sheet. After \mathbf{J} also being second-quantized as the Hamiltonian, we obtain operators J_x and J_y , both of which are composed of the elements of set \mathbb{P} , and do not be exhibited explicitly here due to their complexity.

With σ_{ij} at hand, we could work out the transmission T_r and Faraday rotation angle θ_F of the input optical field E^i using

$$(E_x^i, 0) + (E_x^r, E_y^r) = (E_x^t, E_y^t), \tag{24}$$

and

$$\frac{\partial E_x^t}{\partial z} - \frac{\partial E_x^i}{\partial z} - \frac{\partial E_x^r}{\partial z} = -i\omega_p \mu_v \sum_{j=x,y} \sigma_{ij} E_j^t, \quad z = 0 \tag{25}$$

in which μ_v the vacuum permeability. T_r and θ_F appear in the following forms [23]

$$T_r(\omega_p) = \frac{|t_+|^2 + |t_-|^2}{2\sqrt{\epsilon_g}}, \tag{26}$$

$$\theta_F(\omega_p) = \frac{\theta_- - \theta_+}{2}, \tag{27}$$

where $t_{\pm} = \frac{E_x^t \pm i E_y^t}{E_x^i} = |t_{\pm}| e^{i\theta_{\pm}}$ represent the left and right circular polarizations.

3 Results and discussions

From Fig. 2a, we observe a variety of phenomenon, which are just the same as those in Ref.[18]. These results include a sequence of absorption peaks at the frequencies $E_1/\hbar = 95.4\text{THz}$, $(E_2 - E_{-1})/\hbar = 230.3\text{THz}$, $(E_3 - E_{-2})/\hbar = 300.2\text{THz}$ and the Shubnikov-de Haas oscillations around $\sigma_g = \pi e^2/2h$ [24, 25, 26, 27, 28, 29, 30, 31], which completely justify our hypothesis and treatments. Figure 2b is also analogous to its counterpart in Ref. [18]. Figure 3a, b shows the case for higher electronic density ($E_F = 0.2\text{eV}$). The intraband transitions dominate while the interband transitions are locked at low frequency regime, such as the peaks of σ_{xx} and σ_{xy} at frequencies $\frac{E_{N_F+1} - E_{N_F}}{\hbar} = 14.7\text{THz}$ (N_F is the index of the last Landau level whose energy is smaller than E_F). However, the interband transitions caused Shubnikov-de Haas oscillation appear again at high frequencies ($\geq \frac{E_{N_F+1} + E_{N_F}}{\hbar} = 618.1\text{THz}$). Two interband transitions at $\frac{E_{N_F} - E_{-N_F-1}}{\hbar} = 618.1\text{THz}$ and $\frac{E_{N_F} - E_{-N_F+1}}{\hbar} = 587.9\text{THz}$ introduce two small fluctuations (see the inset of Fig. 3b).

Therefore, it is reasonable to anticipate that a novel viewpoint on graphene can be obtained via our hypothesis. We could see that a monolayer graphene in an external magnetic field can be viewed as an ensemble of tremendously numerous noninteracting TLAs with relatively large frequency-dependent electric dipole moments (in the order of 300 Debye). With this viewpoint, the giant optical nonlinearity and giant Faraday rotation of graphene are expected [18, 32]. In addition to the explanation of the optical properties of graphene, our model also opens up a novel approach for the calculations where the graphene is coupled to other materials such as Au-MNPs.

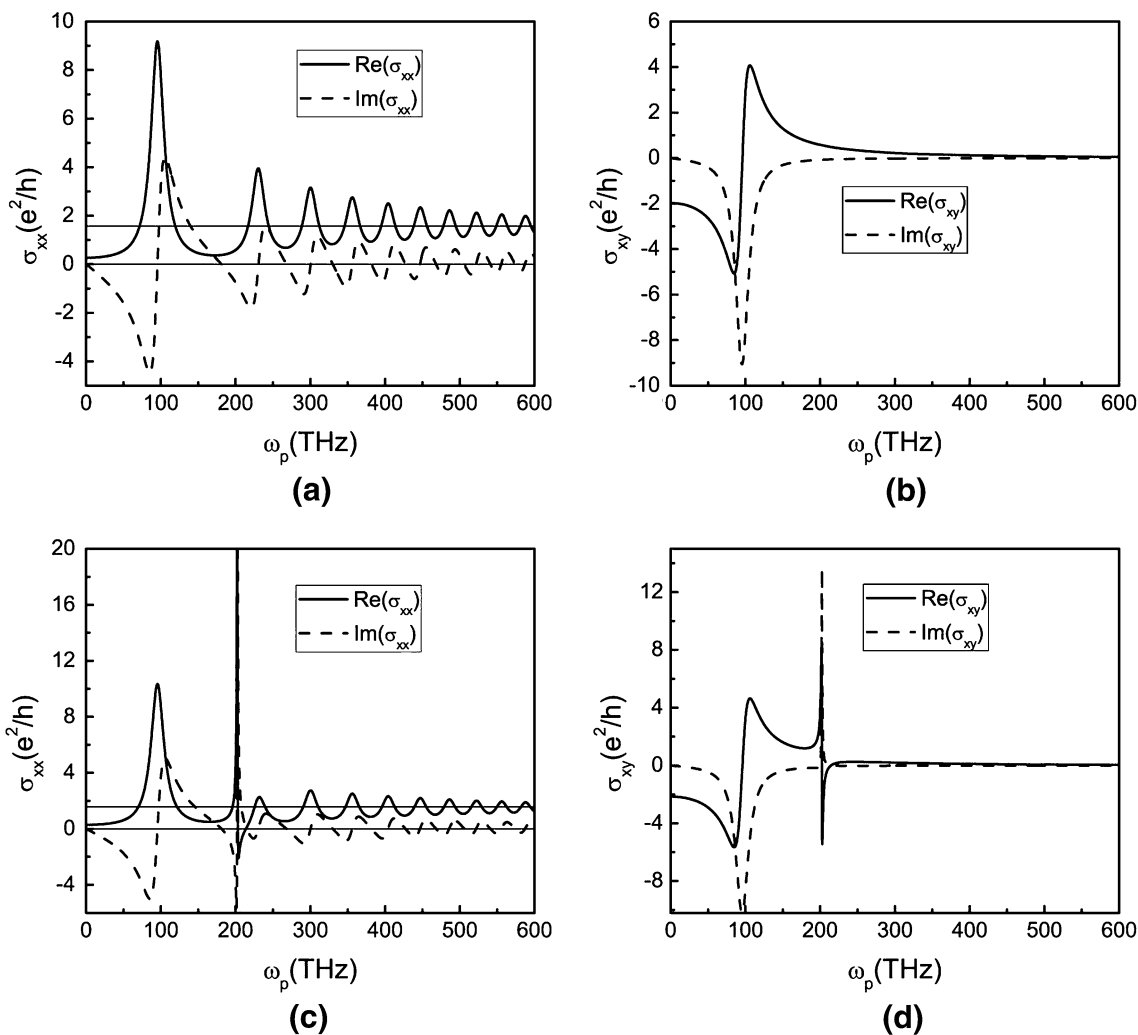


Fig. 2 Longitudinal magneto-optical conductivity as a function of the light beam frequency with $B = 3T$, $T = 20$ K, $\Gamma = 10.5$ THz and Fermi energy $E_F = 0$. The parameters of Au-MNP are $\epsilon_b = \epsilon_g =$

3.9 , $\omega_{spp} = 600$ THz, $\gamma_{spp} = 3$ THz, $r_0 = 5$ nm and $d = 14$ nm. **a, b** indicate the case without the Au-MNP while **c, d** are the case with Au-MNP

Figure 2c, d and Fig. 3c, d demonstrate the influence of Au-MNP on the optical conductivity. A very sharp peak presents in those figures. Those variations bring significant modifications to the usual FRE depicted in Fig. 4. The hallmark of FRE is the rotation angle, which experiences a sudden soar and drop in the narrow vicinity of the frequency at 200 THz when the Au-MNP is present. The value of the sharp peak even exceeds 2° at a relatively high frequency where should have a nearly zero θ_F without Au-MNP. An even more mentionable contrast is found between Fig. 4c, d, i.e., a transmission greater than 100 %. This means that the beam around 200 THz would go through an unusual amplification, indicating an energy flow from Au-MNP to the output beam. This amplification is of great advantage to the detection of FRE and the implementation of optical switches based on it. Furthermore, the

FRE could be adjusted by altering the MNP-graphene distance. According to Fig. 5, the MIFRE will be strengthened provided Au-MNP is moved closer to graphene sheet, which displays the tunability of FRE. All those advantages of MIFRE manifest its better practicality than FRE.

In order to illustrate an insight into the underlying physics of MIFRE, it is suitable just to take $\eta - 1$ (the direct contribution from Au-MNP) into consideration and to ignore the so-called self-interaction term of the TLAs $\mu \zeta S^-$ (according to Ref.[33]) due to its smallness, which could be checked merely with rough calculation. When checking the expression for $\eta - 1$, one would discover that many parameters in it are determined by intrinsic properties of Au-MNP. Except for light beam frequency ω_p , only d , ϵ_b and ϵ_g could be adjusted from outside. Since

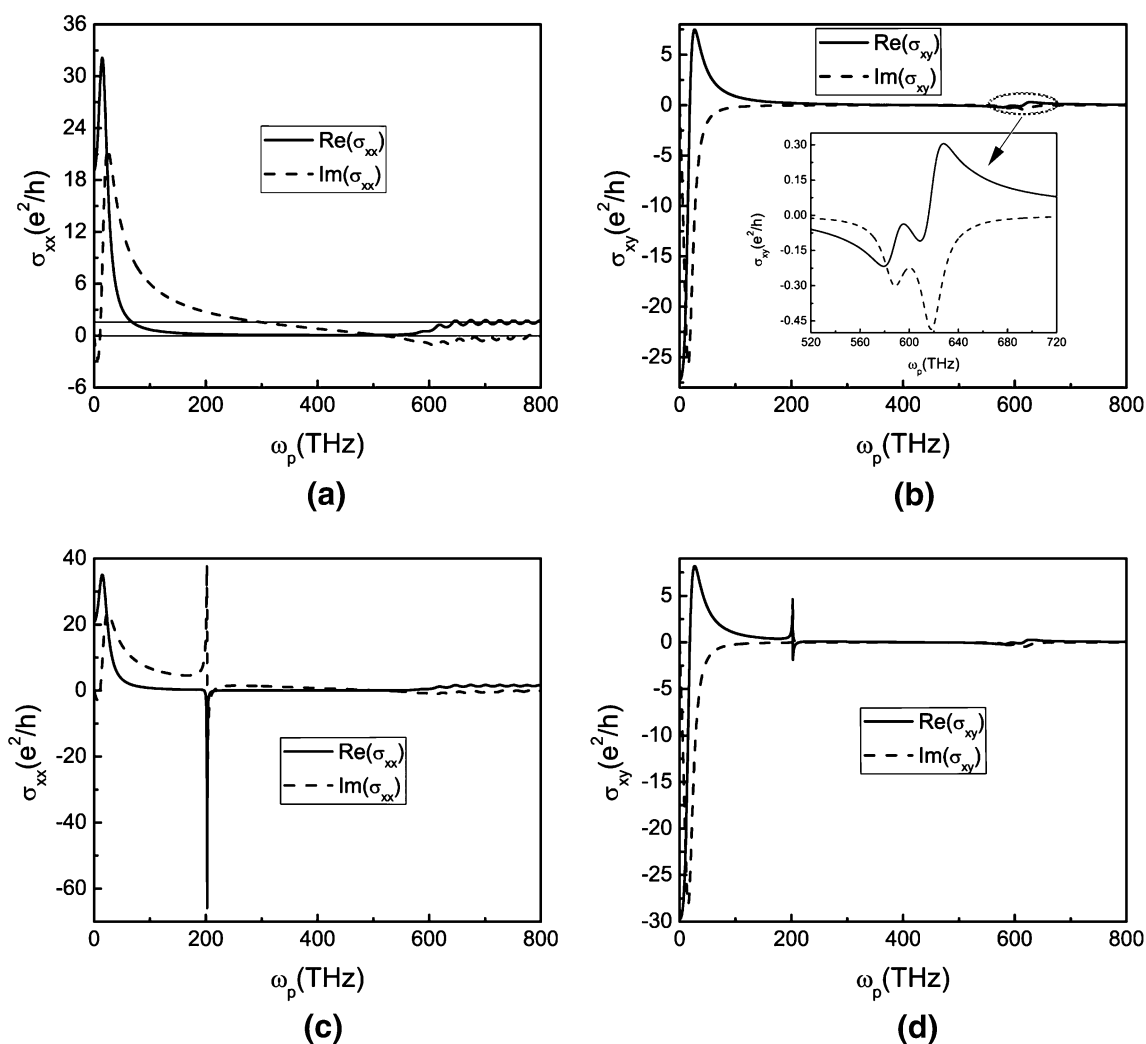


Fig. 3 Longitudinal magneto-optical conductivity as a function of the light beam frequency with Fermi energy $E_F = 0.2\text{eV}$. The other parameters used are the same as those in Fig. 2. **a, b** indicate the case without the Au-MNP while **c, d** are the case with Au-MNP

d will not determine the position of the exotic frequency (see Fig. 5), we mainly focus on the shift of exotic frequency due to ε_b and ε_g (see Fig. 6). From Fig. 6 a, b, one should identify an efficient shift, which provides another method to manipulate MIFRE. Together with this shift, the Au-MNP induced sharp peak of optical conductivities σ_{xx} and σ_{xy} drifts as well (see Fig. 6c, d). The direct contribution from Au-MNP acts as an equivalent input optical field interfering with actual input field and makes a difference to the effective field imposed on graphene. When $|\eta - 1|$ is in its raising stage, the phase of $\eta - 1$ is mostly between 0 and π . This means that the constructive interference should dominate and result in the enhanced optical conductivity. Hence, a strongly modified FRE is expected. But after $|\eta - 1|$ crosses its peak and starts going down, the phase of $\eta - 1$ is mostly around π . Now, the destructive interference is dominant, and the optical conductivity will decrease. Finally, they reach their minimums

and recover a little bit after the minimums owing to the continuously dropping $|\eta - 1|$. The Au-MNP plays the role of “coherent light source” in the process described above.

On the other hand, the Au-MNP could be regarded as the supplier of a stack of almost continuum levels (see the inset of Fig. 6c). This level stack provides the probability of the quantum interference between the two transition processes, i.e., the direct transition and indirect transition via the MNP-graphene (i.e., many TLAs with different energy levels in our model) coupling. The constructive or destructive interference between two competing optical pathways will lead to the peculiar asymmetric lineshape in Fig. 6c, d, which is a Fano-like effect. By decreasing the MNP-graphene distance d , the MNP-graphene coupling and thus the Fano-like effect are strengthened. In this case, a more pronounced asymmetric lineshape is present as shown in Fig. 6d. The quantum interference also makes the overall transition process enhanced or suppressed, leading

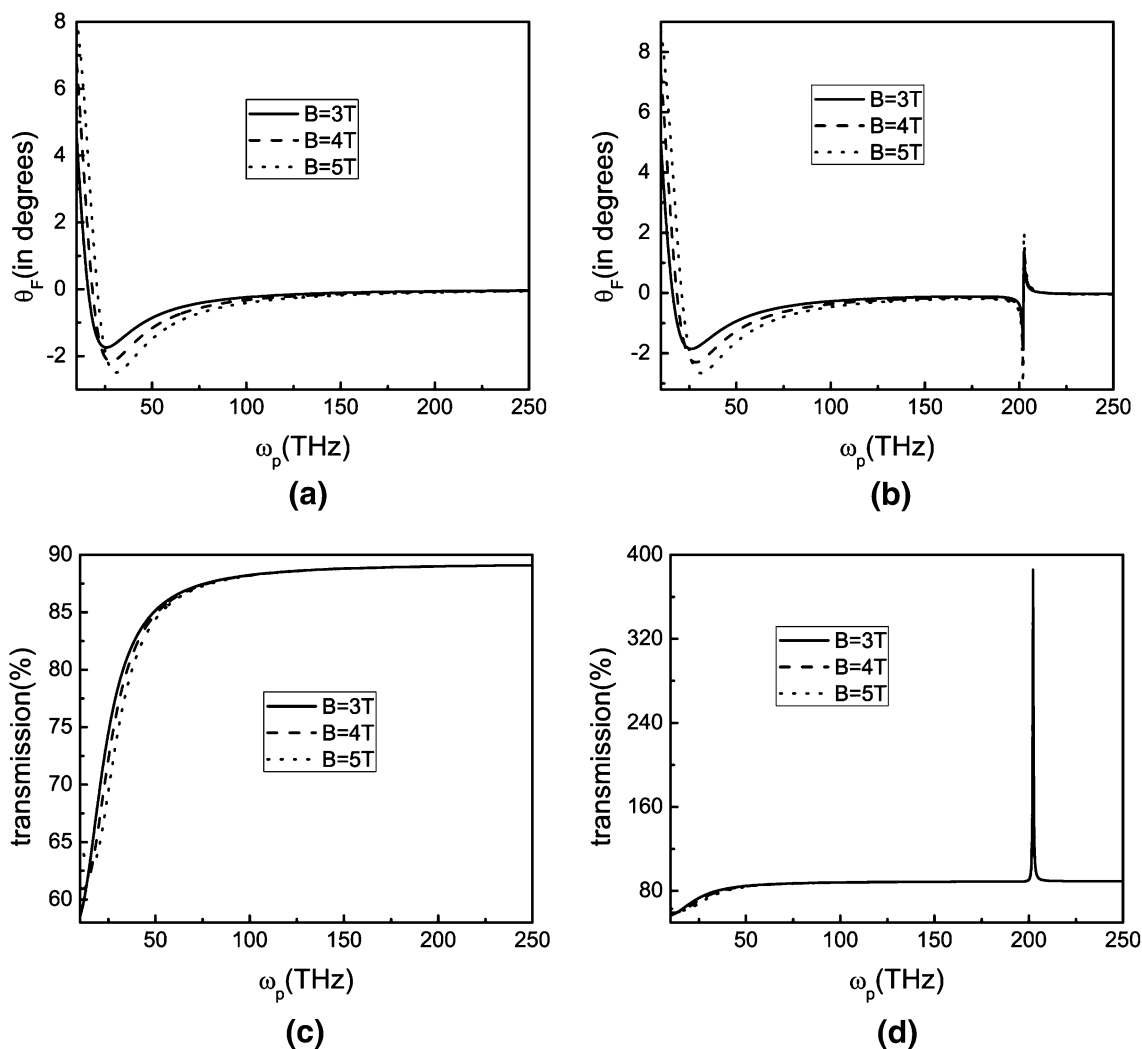


Fig. 4 Transmission and Faraday rotation angle θ_{IF} (in degrees) of the light beam as a function of the beam frequency with $E_{IF} = 0.3\text{eV}$ and different magnetic fields. The other parameters used are the same

as those in Fig. 2. **a, c** indicate the case without the Au-MNP while **b, d** are the case with Au-MNP

to the increased or decreased optical conductivities and FRE. When the light beam is at the frequency relatively far away from the “coherent resonance frequency” of Au-MNP, the MNP-graphene coupling is so weak that no effective indirect transition path could be established. Thus, no quantum interference will appear. In this case, the MIFRE and Fano-like effect will both disappear. However, only when the beam frequency is around the resonance frequency, these phenomena will be happened owing to the strong enough MNP-graphene coupling. It is obvious that Fano-like effect and MIFRE will occur and vanish simultaneously. Therefore, one may say that both of the MIFRE and Fano-like effect really stem from the MNP-graphene coupling.

The interesting phenomena induced by Au-MNP in graphene should not be limited to MIFRE. As an instance, we investigate the static Hall conductivity $\sigma_{xy}(\omega_p \rightarrow 0)$. The Hall conductivity quantization rule of graphene reads

$$\sigma_{xy}(0) = -\frac{4e^2}{h} \left(N_F + \frac{1}{2}\right). \tag{28}$$

This equation has been indicated in Fig. 7. The widths of the plateaus is determined by the distances between LLs. The step height is $\Delta_0 = 4e^2/h$. When the Au-MNP is present, the step height will be changed with the widths of the plateaus unaffected. The Hall conductivity quantization rule of graphene now could be expressed as

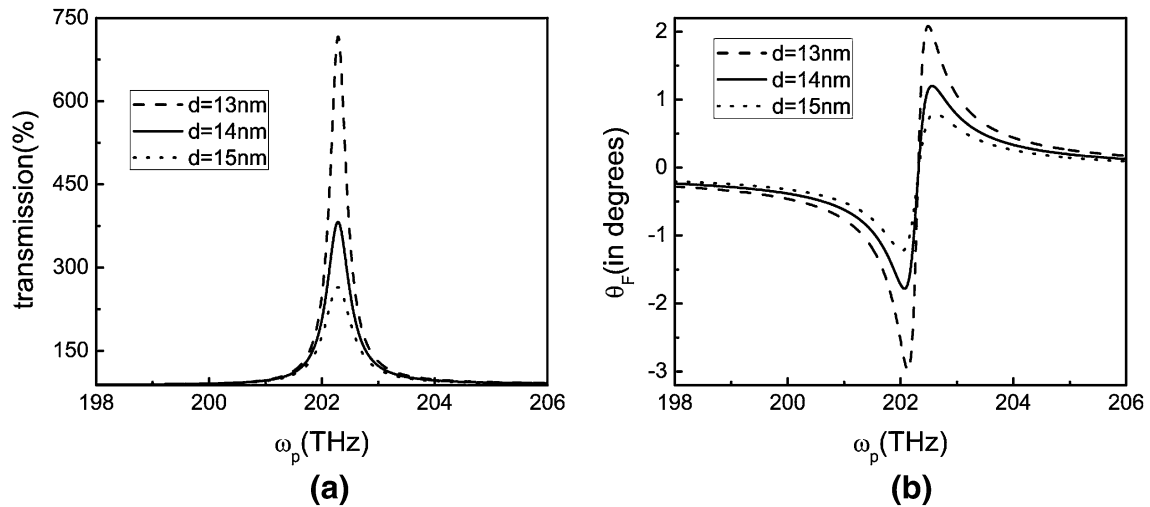


Fig. 5 Transmission and Faraday rotation angle θ_F (in degrees) of the light beam whose frequency is around the exotic point due to Au-MNP. $E_F = 0.3$ eV and the other parameters used are the same as those in Fig. 2

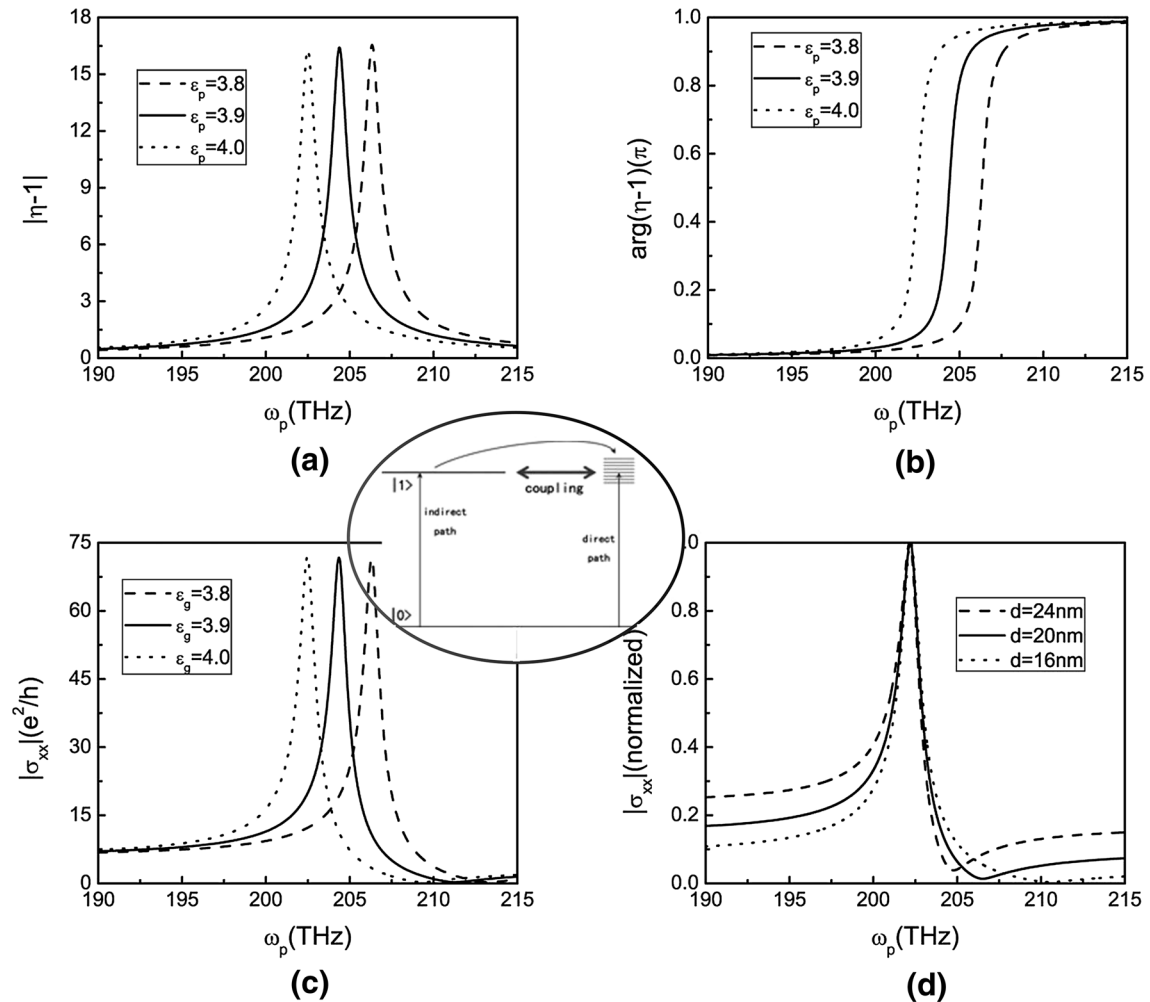


Fig. 6 $|\eta-1|$, $\arg(\eta-1)$ and absolute value of $|\sigma_{xx}|$ as functions of the beam frequency ω_p with different ϵ_g ($\epsilon_g = \epsilon_b$, $d = 20$ nm, **a**, **b** **c**) and different graphene-MNP distance d ($\epsilon_g = \epsilon_b = 3.9$, **d**). The other parameters used are the same as those in Fig. 2 except for $E_F = 0.3$ eV.

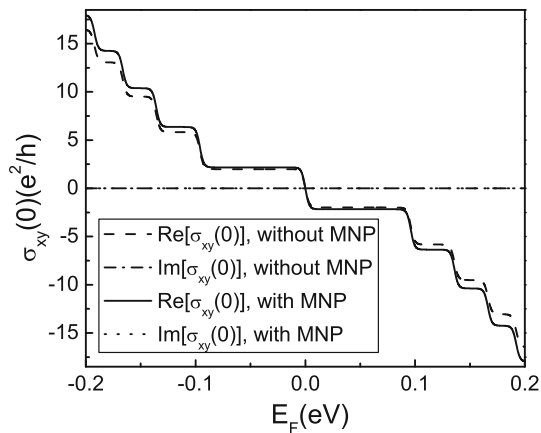


Fig. 7 The static Hall conductivity as a function of Fermi energy. The other parameters used are the same as those in Fig. 2 except for $B = 7T$

$$\sigma_{xy}(0) = -\eta \frac{4e^2}{h} \left(N_F + \frac{1}{2} \right). \quad (29)$$

Then, Δ_0 should be $4\eta e^2/h$, meaning that Δ_0 could be tuned by adjusting Au-MNP. This property is introduced completely from an outside source, i.e., Au-MNP.

4 Conclusion

In conclusion, we have investigated how a MNP affects the Faraday rotation effect in graphene and have found the MIFRE phenomena. The MIFRE is typically strong due to the MNP-graphene coupling and could be tuned by adjusting the MNP-graphene distance and the dielectric constants. The Au-MNP-induced modifications on Hall conductivity has also been demonstrated. During the calculations, we proposed a novel model on the monolayer graphene sheet in an external magnetic field. This model offers a clear physical understanding of the optical properties of graphene and a convenient way to compute more complex systems involving graphene. We expect that the MIFRE could be realized experimentally in the future, and more interesting phenomenon could be revealed with our method.

Acknowledgments This study was supported by the National Natural Science Foundation of China (Nos. 10974133 and 11274230) and the Ministry of Education Program for PhD.

References

1. A. Ridolfo, O. Di Stefano, N. Fina, R. Saija, S. Savasta, *Phys. Rev. Lett.* **105**, 263601 (2010)
2. R.D. Artuso, G.W. Bryant, A. Garcia-Etxarri, J. Aizpurua, *Phys. Rev. B* **83**, 235406 (2011)
3. I. Mukherjee, G. Hajisalem, R. Gordon. *Opt. Express* **19**, 22462 (2011)
4. J.Y. Lee, P. Peumans. *Opt. Express* **18**, 10078 (2010)
5. H.Y. Lin, C.H. Huang, C.H. Chang, Y.C. Lan, H.C. Chui. *Opt. Express* **18**, 165 (2010)
6. R.D. Artuso, G.W. Bryant. *Phys. Rev. B* **87**, 125423 (2013)
7. S.G. Kosionis, A.F. Terzis, S.M. Sadeghi, E. Paspalakis. *J. Phys. Condens. Matter* **25**, 045304 (2013)
8. W.J. Hong, H. Bai, Y.X. Xu, Z.Y. Yao, Z.Z. Gu, G.Q. Shi. *J. Phys. Chem. C* **114**, 1822 (2010)
9. Y. Wang, S.J. Zhen, Y. Zhang, Y.F. Li, C.Z. Huang. *J. Phys. Chem. C* **115**, 12815 (2011)
10. Y. Li, X.B. Fan, J.J. Qi, J.Y. Ji, S.L. Wang, G.L. Zhang, F.B. Zhang. *Nano. Res.* **3**, 429 (2010)
11. A.M. Zaniewski, M. Schriver, J.G. Lee, M.F. Crommie, A. Zettl. *App. Phys. Lett.* **102**, 023108 (2013)
12. P.S. Pershan. *J. Appl. Phys.* **38**, 1482 (1967)
13. S.A. Wolf. *IBM J. Res. Dev.* **50**, 101 (2006)
14. I. Crassee, J. Levallois, A.L. Walter, M. Ostler, A. Bostwick, E. Rotenberg, T. Seyller, D.V. d. Marel, A.B. Kuzmenko. *Nature Physics* **7**, 48 (2011)
15. I. Fialkovsky, D.V. Vassilevich. *Eur. Phys. J. B* **85**, 384 (2012)
16. A. Fallahi, J. Perruisseau-Carrier. *App. Phys. Lett.* **101**, 231605 (2012)
17. N. Ubrig, I. Crassee, J. Levallois, I. O. Nedoliuk, F. Fromm, M. Kaiser, T. Seyller, A. B. Kuzmenko, <http://arxiv.org/abs/1303.1634> (2013)
18. A. Ferreira, J. Viana-Gomes, Y.V. Bludov, V. Pereira, N.M.R. Peres, A.H. Castro Neto. *Phys. Rev. B* **84**, 235410 (2011)
19. W. Zhang, A.O. Govorov, G.W. Bryant. *Phys. Rev. Lett.* **97**, 146804 (2006)
20. J.Y. Yan, W. Zhang, S. Duan, A.O. Govorov. *Phys. Rev. B* **77**, 165301 (2008)
21. N.M.R. Peres. *Rev. Mod. Phys.* **82**, 2673 (2010)
22. J.W. McClure. *Phys. Rev.* **104**, 666 (1956)
23. R.F. O'Connell, G. Wallace. *Phys. Rev. B* **26**, 2231 (1982)
24. N.M.R. Peres, F. Guinea, A.H. Castro Neto. *Phys. Rev. B* **75**, 125411 (2006)
25. T. Ando, Y. Zheng, H. Suzuura. *J. Phys. Soc. Jnp.* **71**, 1318 (2002)
26. V.P. Gusynin, S.G. Sharapov. *Phys. Rev. B* **73**, 245411 (2006)
27. V.P. Gusynin, S.G. Sharapov, J.P. Carbotte. *Phys. Rev. Lett.* **96**, 256802 (2006)
28. L.A. Falkovsky, S.S. Pershoguba. *Phys. Rev. B* **76**, 153410 (2007)
29. L.A. Falkovsky, A.A. Varlamov. *Eur. Phys. J. B* **56**, 281 (2007)
30. T. Stauber, N.M.R. Peres, A.K. Geim. *Phys. Rev. B* **78**, 085432 (2008)
31. N.M.R. Peres, T. Stauber. *Int. J. Mod. Phys. B* **22**, 2529 (2008)
32. X.H. Yao, A. Belyanin. *Phys. Rev. Lett.* **108**, 255503 (2012)
33. R.D. Artuso, G.W. Bryant. *Nano. Lett.* **8**, 2106 (2008)